ACS APPLIED MATERIALS & INTERFACES

Research Article

Cite This: ACS Appl. Mater. Interfaces 2019, 11, 11857−11864

www.acsami.org

Protein−Inorganic Hybrid Nanoflower-Rooted Agarose Hydrogel Platform for Point-of-Care Detection of Acetylcholine

Deshuai Kong,[†] Rui Jin,[†] Xu Zhao,[†] Hongxia Li,[†] Xu Yan,*[,†] Fangmeng Liu,[†] Peng Sun,[†] Yuan Gao,[†] Xishuang Liang,[†] Yuehe Lin,[‡] and Geyu Lu*[,†]

[†]State Key Laboratory on Integrated Optoelectronics, College of Electronic Science and Engineering, Jilin University, Changchun 130012, People's Republic of China

[‡]School of Mechanical and Materials Engineering, Washington State University, Pullman, Washington 99164, United States

Supporting Information

ABSTRACT: Rapid and precise profiling of acetylcholine (ACh) has become important for diagnosing diseases and safeguarding health care because of its pivotal role in the central nervous system. Herein, we developed a new colorimetric sensor based on protein−inorganic hybrid nanoflowers as artificial peroxidase, comprising a test kit and a smartphone reader, which sensitively quantifies ACh in human serum. In this sensor, ACh indirectly triggered the substrate reaction with the help of a multienzyme system including acetylcholinesterase, choline oxidase, and mimic peroxidase (nanoflowers), accompanying the enhancement of absorbance intensity at 652 nm. Therefore, the multienzyme platform can be used to detect ACh via monitoring the change of the absorbance in a range from 0.0005 to 6.0 mmol L^{-1}. It is worth mentioning that the platform was used to prepare a portable agarose gel-based kit for rapid qualitative monitoring of ACh. Coupling with ImageJ program, the image information of test kits can be transduced into the hue parameter, which provides a directly quantitative tool to identify ACh. Based on the advantages of simple operation, good selectivity, and low cost, the availability of a portable kit for point-of-care testing will achieve the needs of frequent screening and diagnostic tracking.

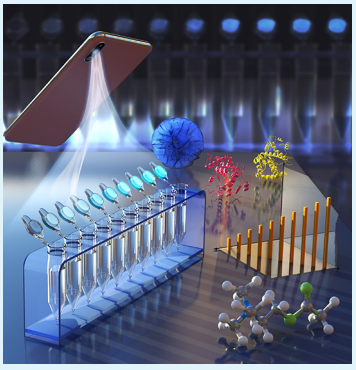

KEYWORDS: *protein−inorganic hybrid nanoflowers, portable kits, point-of-care, nanozyme, acetylcholine*

1. INTRODUCTION

Acetylcholine (ACh), which plays a vital role in learning,[1] memory,[2] exercise,[3] mood,[4] and other biological fields,[5,6] is always a participant involved in the central nervous system and other peripheral nervous systems[7,8] as neurotransmitters to deliver signals. If the amount of ACh in the body is no longer within the normal range, it can affect the termination of synaptic transmission of neurotransmitters that are highly related to Alzheimer's disease,[9] Parkinson's disease,[10] progressive dementia,[11] schizophrenia,[12] and motor dysfunction.[13] Driven by the above facts, many researchers focus on the detection of ACh to identify diseases in its early stage. Simultaneously, the research of ACh in biological samples is of great significance in the research of functional and physiological aspects of neural disorders.[14,15] Thus, various sensing assays have been reported for ACh detection including high-performance liquid chromatography,[16,17] optical detection,[18,19] and electrochemistry.[20,21] Although these test approaches are promising, they are always expensive and time-consuming, especially the requirement of skilled workers to perform these experiments in well-equipped laboratories, which could not satisfy the needs of on-site detection and simplified experimental steps to reach a wider range of applications. Therefore, it is the priority to fabricate a portable and rapid visual detection strategy for ACh. Now, colorimetry displays a great potential in biological analysis, thanks to its high stability and great convenience. Through previous reports, colorimetry was found to be used in the detection of other materials such as DNA,[22] glucose[23]-converting enzyme,[24] and dopamine.[25] The availability of on-site colorimetric biosensors will make frequent screening and diagnosis possible.[26,27]

Recently, imitative enzyme nanomaterials (defined as nanozyme) as one of the promising nanomaterials have been widely used in colorimetry with extraordinary catalytic efficiency.[28,29] Because of their affordable, high stability, simple preparation, and tunable catalytic activity, nanozymes have been employed as an ideal substitute of natural enzyme for on-site detection. For example, some inorganic nanomaterials have been found to take on intrinsic enzymatic activities,[30] such as gold nanoparticles,[31] Fe_3O_4,[32] CeO_2,[33] and graphene oxide.[34] At present, the research on many organic nanomaterials has further expanded the variety of imitation of the enzyme catalysts, which have broad prospects in environmental detection and biomedicine as the imitation of enzyme technology.[35] As a kind of advanced nanometer materials, protein−inorganic hybrid nanoflowers with flowerlike hier-

Received: December 10, 2018
Accepted: March 4, 2019
Published: March 4, 2019

DOI: 10.1021/acsami.8b21571
ACS Appl. Mater. Interfaces 2019, 11, 11857−11864

archical structures possessed unique peroxidase catalytic activity.[36] Nanoflowers can integrate different components including metal ions (Ca^{2+}, Co^{2+}, Cu^{2+}, Mn^{2+}, etc.), antibodies, enzymes, and other biomolecules, spontaneously through the self-assembly to achieve the required hybrid materials.[37] Previous studies showed that copper-based nanoflowers could serve as a reagent similar to Fenton's reagent in an acidic environment, catalyzing the substrate to produce colored products.[38]

Inspired by the above development, we herein set up a colorimetric system for the visual detection of ACh based on organic−inorganic hybrid nanoflowers that take protein as a template (Scheme 1). In our work, bovine serum albumin

Scheme 1. Illustration of Self-Assembled Nanoflowers and the Corresponding Scheme for the Detection of ACh

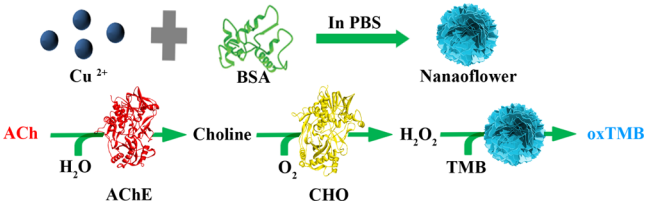

(BSA)−$Cu_3(PO_4)_2{\cdot}3H_2O$ nanoenzyme with a mimic peroxidase activity could catalytically convert 3,3′,5,5′-tetramethylbenzidine (TMB) which is oxidized to oxTMB in the presence of H_2O_2.[39,40] The concentration about H_2O_2 was controlled by ACh-triggered enzymatic reaction of acetylcholinesterase (AChE) and choline oxidase (CHO). Thus, the changing of absorbance produced the corresponding signal to accurately detect ACh. Because of cheap and readily available compared to ferrocene−phenylalanine hydrogels and guanosine−borate hydrogels,[41,42] agarose hydrogels as a proficient on-site operational solid sensing platform were further used to design a portable tool for ACh visual inspection, and successfully applied to the determination of for profiling ACh level in human serum.

2. EXPERIMENTAL SECTION

2.1. Reagents and Instruments. All chemicals were used as received without further purification. H_2O_2, NaOH, cupric sulfate ($CuSO_4$), sodium phosphate monobasic anhydrous (NaH_2PO_4), and sodium phosphate dibasic anhydrous (Na_2HPO_4) were bought from Sinopharm Chemical Reagent Co., Ltd. (Shanghai, China). Horse radish peroxidase (HRP), trypsin (TRY), glutathione (GSH), BSA, threonine (THR), aspartic acid (ASN), L-phenylalanine (L-PHE), histidine (HIS), arginine (ARG), glycine (GLY), glucose oxidase (GOX), and TMB were bought from Aladdin Reagent Co., Ltd. (Shanghai, China). ACh, AChE (0.2 U mg^{-1}), and CHO (8.0 U mg^{-1}) were bought from Ryon Biological Technology Co., Ltd. (Shanghai, China). Acetate buffer solution and Tris-HCl buffer solution were acquired from Sigma-Aldrich reagent Co., Ltd. (St. Louis, MO, USA).

The UV−vis absorbance was measured by a UV-2550 spectrometer (Shimadzu). The morphological structures were observed by JEM-7500 TEM (JEOL, Japan) and JEM-2100 field emission scanning electron microscopy (SEM) (JEOL, Japan).

2.2. Synthesis of Organic−Inorganic Hybrid Nanoflowers. Nanoflowers were prepared according to the previous literature.[47] Nanoflowers were synthesized perfectly when 200 mmol L^{-1} $CuSO_4$ were added to phosphate-buffered saline (PBS) at pH 6.8 containing 0.1 mg mL^{-1} BSA and 845 μL of deionized water. After standing for 12 h at room temperature, the obtained nanoflowers were purified by washing two times with deionized water. The precipitation was diluted to 100 μL with PBS and stored in 4 °C for further use.

2.3. Steady-State Kinetics. A 100 μL of different concentrations of H_2O_2 and 50 μL of nanoflowers were added into the substrate solution containing 150 μL of NaAc buffer solution, 50 μL of TMB, and 1650 μL of deionized water at room temperature. After being reacted with for 30 min, UV−vis absorptions were measured at 652 nm. The apparent steady-state kinetic parameters for the catalytic oxidation of substrates by nanoflowers were detected through using the Beer−Lambert law at the kinetics mode of UV−vis spectrophotometer (UV-2550). Kinetic experiments carried out by using nanoflowers in an NaAc buffer (pH = 4.0) contain 100 mmol L^{-1} H_2O_2 as a substrate and different concentrations of TMB (0.01−1.2 mmol L^{-1}). In addition, the kinetics were investigated in variable H_2O_2 concentrations (0.2−80 mmol L^{-1}) with a constant TMB concentration (1.0 mg mL^{-1}).

2.4. Determination of ACh. 1.0 U mL^{-1} of AChE (50 μL) and 2.0 U mL^{-1} of CHO (50 μL) were added to 100 μL of different concentrations of ACh in Tris-HCl buffer solution (pH = 8.0). After 30 min of incubation, 150 μL of nanoflowers, 1.0 mg mL^{-1} of TMB (50 μL), and 100 mmol L^{-1} of NaAc buffer (150 μL, pH 4.0) were reacted for 30 min at room temperature. The UV−vis absorptions were measured at 652 nm.

2.5. Real Sample Detection. The colorimetry was used to detect ACh in human serum and evaluate its applicability. The affiliated hospital of Jilin University (Changchun, China) provided us with the

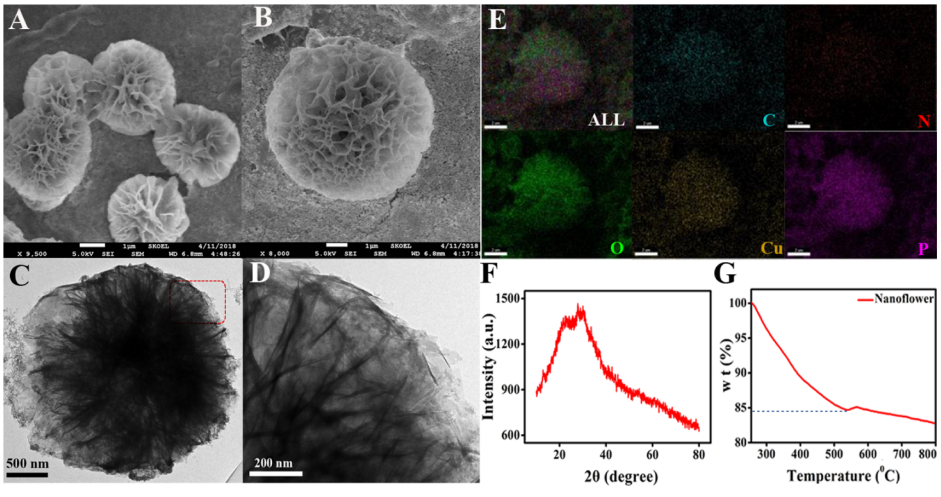

Figure 1. SEM (A,B), TEM (C,D), EDX (E), XRD (F), and thermogravimetric analysis (G) of nanoflowers.

DOI: 10.1021/acsami.8b21571
ACS Appl. Mater. Interfaces 2019, 11, 11857−11864

healthy human blood. The experiment was conducted in accordance with the professional ethics relevant to legal and institutional guidelines. Because of the high content of protein in plasma, some pretreatment methods were used to eliminate the interference of coexisting substances. The treatment steps were as follows: the human blood was immobilized for 2 h to obtain the upper serum. The serum samples were diluted 60 times with deionized distilled water. In the recovery study, a certain amount of ACh standard was added to the sample before pretreatment with the described method.

2.6. Fabrication of Portable Kit. Portable ACh detection kits were prepared: 20 mg of agarose was added into 100 °C boiling water. When the solution fell to 40 °C, 200 μL of nanoflower solution, 75 μL of TMB (1.0 mg mL^{-1}), and 250 μL of NaAc buffer (100 mmol L^{-1}) were added into the solution. After blending, 200 μL of the mixed solution was dropped to the top tube. The test kits were stored in 4 °C for further use. For ACh detection, 50 μL of AChE (1.0 U mL^{-1}) and 50 μL of CHO (2.0 U mL^{-1}) were mixed with Tris-HCl buffer solution with a pH of 8.0. Then, 100 μL of ACh was added to the test system. The cap was closed and the test kit was kept upside down for the sample solution penetration into water gel in 37 °C for 30 min. Depending on the concentration of ACh in the sample solution, the color range of the hydrogel varies from colorless to blue. Then, ACh was dissolved into the serum and the above operation was performed again. Furthermore, the stability of the kit was investigated for 15 consecutive days.

3. RESULTS AND DISCUSSION

3.1. Characterization of Nanoflowers. Inspired by the biomineralization process, BSA was simply placed into the Cu^{2+}/PO_4^{3-} solution at room temperature for the preparation of BSA–$Cu_3(PO_4)_2{\cdot}3H_2O$ hybrid nanoflowers. After 12 h reaction, it is notable to observe that the blue precipitate was obtained. This method is simple and easy to operate, without toxic elements and complex purification process. To investigate the morphology, SEM images of the hybrid materials are demonstrated in Figure 1A. It was found that the hybrid products had hierarchical structures with a flowerlike nanostructure, which seem similar to those composed of a large number of interlaced nanopetals. The three-dimensional layered structure of the nanoflowers effectively increases the specific surface area of the nanoflowers, improves the recognition of the substrates, and thus improves the biocatalytic activity of the nanoflowers. As can be seen from Figure S1A, the structure of the nanosheet with a diameter about 500 nm (Figure S1B) was formed at the secondary hour when the biomineralization process happened, indicating that the nanoflowers were not fully formed. After 12 h reaction, these nanosheets are stacked to form flower structures with relative uniformity, which looks similar to hydrangeas with an average size of 5.0 μm (Figure 1B). Transmission electron microscopy (TEM) image further revealed the flower morphology (Figure 1C) with a branchlike structure, which were composed of nanosheet structures (Figure 1D). The image of energy-dispersive X-ray (EDX) detector showed that five typical elements including C, N, O, P, and Cu were observed in the nanoflowers and attributed to $Cu_3(PO_4)_2$ and BSA components. Thus, the nanoflowers using BSA as the template and $Cu_3(PO_4)_2{\cdot}3H_2O$ as the skeleton, proved that nanoflowers have successfully carried the protein (Figure 1E). The X-ray diffraction (XRD) pattern of the nanoflowers were also basically consistent with the previous literature[37] (Figure 1F). Biocompatible $Cu_3(PO_4)_2$ plays a vital role in the immobilization of BSA. The load-carrying capacity of hybrid nanoflowers was measured by thermogravimetric analysis (Figure 1G). Remarkably, the nanoflower levels began to decrease after 250 °C, and the proteins began to burn to ash, eventually leaving about 82% of the original solids. In other words, the proportion of protein in the nanoflowers is 18%, indicating that the protein had successful loading in our nanoflowers. Therefore, all of these consequences indicated that the protein–inorganic hybrid nanoflowers were successfully prepared.

3.2. Catalytic Ability of Nanoflowers. After the successful preparation of hybrid nanomaterials, the mimic peroxidase activity was further investigated. To verify the catalytic performance, nanoflowers acted on the substrate (TMB and H_2O_2) to produce a redox reaction. As depicted in Figure 2A, control experiments revealed that no obvious

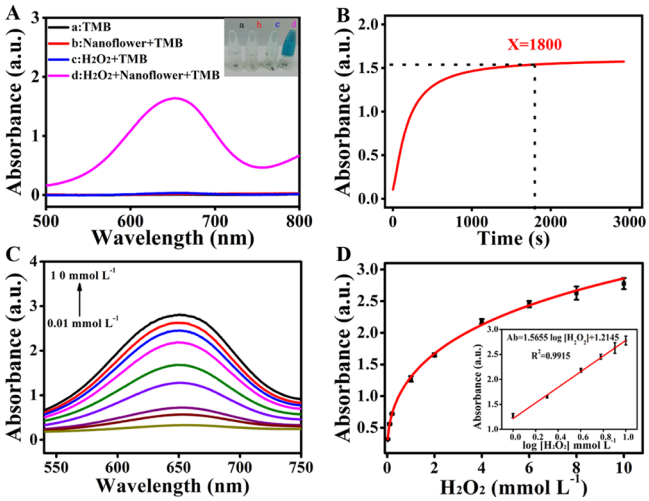

Figure 2. (A) UV–vis absorption curves of reaction solutions: blank control (a), nanoflowers (b), H_2O_2 (c), and nanoflowers + H_2O_2 (d). The illustration shows the corresponding color change in response. (B) Kinetic analysis of system toward H_2O_2. (C) UV–vis absorption of different concentration of H_2O_2 (from 0.01 to 5.0 mmol L^{-1}). (D) Different concentrations of H_2O_2 changes lead to changes in absorbance intensity. The illustration shows excellent linearity between different concentrations of H_2O_2 (0.01, 0.05, 0.1, 0.5, 1.0, 2.0, 3.0, 4.0, and 5.0 mmol L^{-1}) and absorbance intensity. The concentrations of nanoflowers and TMB were 4.0 and 1.0 mg L^{-1}, separately.

absorption peaks appeared between 500 and 800 nm with the single TMB solution (curve a) and TMB solution containing nanoflowers (curve b) or H_2O_2 (curve c), separately. After mixing H_2O_2, nanoflowers, and TMB, the solution showed a significant UV–vis characteristic peak at 652 nm (curve d), guaranteeing that nanoflowers possessed peroxidase-like activity. Simultaneously, the corresponding solution colors changed from colorless to blue (Figure 2 inset). As is known to all, the incubation time plays a vital part in the enzymatic activity reaction. As shown in Figure 2B, the absorbance intensity increased in accordance with the incubation time in a certain range, and the reaction was almost completed with 1800 s. To further verify the catalytic ability of nanoflowers, different amounts of H_2O_2 were catalyzed by fixed concentration of nanoflowers, and then UV–vis absorption of the reaction was measured. Along with the H_2O_2 concentrations increasing from 0.01 to 10 mmol L^{-1}, the absorbance intensity gradually enhanced (Figure 2C). Meanwhile, Figure 2D illustrates a wonderful linear relationship (R^2 = 0.9915) between the concentration of H_2O_2 and the absorbance

DOI: 10.1021/acsami.8b21571
ACS Appl. Mater. Interfaces 2019, 11, 11857–11864

intensities. These results demonstrated the high peroxidase-like catalytic activity of protein−inorganic hybrid nanoflowers.

Furthermore, the catalytic mechanism and the catalytic activities of nanoflowers were investigated by steady-state kinetic analysis. As shown in Figure S2A,B, it showed characteristic Michaelis−Menten behavior toward both H_2O_2 and TMB substrates with the Beer−Lambert law. The values of V_{max} (Maximum reaction rate) and K_m (Michaelis constant) were acquired by linear-fitting analysis method (Figure S2C,D), which was based on the Michaelis−Menten eq 1

$$1/\nu = (K_m/V_{max}) \times (1/[S]) + 1/V_{max} \quad (1)$$

where ν represents the initial velocity, K_m is the symbol of Michaelis−Menten constant, V_{max} represents the maximal reaction velocity, and the [S] is the concentration of the substrate. The results indicated that the K_m of the nanoflowers for H_2O_2 was lower than that of HRP. K_m usually utilized to estimate the binding affinity: a lower K_m value reveals a stronger affinity between the enzyme and substrates. The data showed that the nanoflowers had a relatively higher affinity to H_2O_2 and TMB than natural enzyme (HRP) did (Table 1).

Table 1. Comparison of the Kinetic Parameters of Nanoflowers and HRP[a]

catalyst	substrate	K_m [mM]	V_{max} [M S^{-1}]	references
nanoflower	TMB	0.1709	9.97×10^{-8}	this work
	H_2O_2	1.0014	6.25×10^{-8}	
HRP	TMB	0.434	10.00×10^{-8}	32
	H_2O_2	3.7	8.71×10^{-8}	

[a] K_m is the Michaelis constant, and V_{max} is the maximal reaction velocity.

The high enzymatic activity may be ascribed to the specific surface area of the nanoflowers, which can increase the probability of collision between substrates and active sites, so as to improve the catalytic efficiency.

It is well-known that enzyme catalytic activity is related to reaction conditions. Similar to HRP, the temperature mainly affects the catalytic bioactivity. The effect of temperature on enzyme catalytic activity was first studied. In the range of 4−80 °C (Figure 3A), it had been found that the HRP catalytic activity at 37 °C was the best, but at other temperatures, the activity was inhibited or even completely deactivated at 70 °C. By contrast, the as-prepared nanoflowers had a certain ability of resistance to high temperature, even in 70 °C. These data showed that the proposed nanoflowers had a good thermal stability and could achieve catalytic reaction under high-temperature conditions. This advantage makes the nanoflower materials in the application part with a greater temperature threshold range. More importantly, the 30 day control experiment of nanoflowers and HRP enzyme activity indicated that the catalytic activity of nanoflowers almost did not decrease with the time changing within 30 days, whereas the HRP activity almost completely disappeared on the 3rd day (Figure 3B). The results demonstrated that nanoflowers could be preserved at room temperature for a long time, and their activity remained unchanged. Compared with HRP, the hybrid nanoflowers had better stability, which was the biggest advantage of nanozymes, guaranteeing that it could be served as promising candidates for practice applications.

3.3. Performance for ACh Detection. To achieve a sensitive colorimetric strategy for detecting ACh, a bioassay-

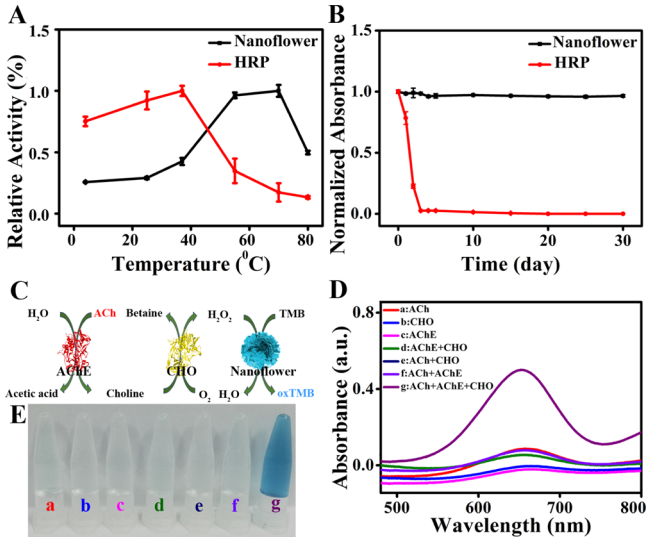

Figure 3. (A) Activities of nanoflowers and HRP were compared at different temperatures. (B) Storage stability of HRP and nanoflowers at room temperature for 30 days. The maximum value observed during each test was set as 100%. (C) Enzyme-cascade-amplification strategy for ACh. (D) UV−vis absorption spectra nanoflower/TMB system in the presence of ACh (a), CHO (b), AChE (c), AChE + CHO (d), ACh + CHO (e), ACh + AChE (f), and ACh + AChE + CHO (g). (E) Corresponding color change of D.

level platform of AChE/CHO was established. AChE enzymatically hydrolyzed ACh to yield choline and catalytically oxidized by CHO to yield betaine and H_2O_2 in the presence of dissolved oxygen (Figure 3C). Subsequently, the formed H_2O_2 was catalyzed to generate hydroxyl radicals by nanoflowers. The hydroxyl radical with a strong electron sensitivity and oxidation ability is easy to oxidize the color substrate. For the feasibility test for monitoring ACh, the absorbance intensity under different circumstances was investigated. As depicted in Figure 3D, these control experiments revealed that no clear absorption peaks appeared between 500 and 800 nm when the solution contains ACh (curve a), CHO (curve b), AChE (curve c), AChE and CHO (curve d), ACh and CHO (curve e), or ACh and AChE (curve f) separately. Only for the mixture of ACh, AChE, and CHO (curve g) at 37 °C, the solution showed a strong characteristic absorption peak at 652 nm. Simultaneously, the corresponding solution color changed from colorless to blue (Figure 3E). On the basis of the above results, the established protocol was feasible for the detection of ACh.

Experimental conditions, such as time, pH value, and temperature, were optimized to obtain good performance for ACh detection. As the pH changed from 7.0 to 8.0, the absorbance of the system remarkably increased, whereas the obvious decreasing of the absorbance appeared with the pH value further increasing to 10.0. Thus, the optimal pH value for AChE/CHO enzymatic activity was at 8.0 (Figure S3A). The influence of the reaction temperature on AChE/CHO enzymatic system is depicted in Figure S3B. With the increasing temperature, the absorbance intensity of the system changed and reached a maximum value at 37 °C. Then, the value slightly decreased with the increasing temperature. Therefore, the optimal temperature for the ACh sensing system is 37 °C. The incubation time (the reaction time of ACh, AChE, and CHO) which had a remarkable influence on

DOI: 10.1021/acsami.8b21571
ACS Appl. Mater. Interfaces 2019, 11, 11857−11864

the system was studied in pH 8.0 Tris-HCl buffer at 37 °C. As shown in Figure S3C, the absorbance had a significant increment with the increasing incubation time. Then, the system reached a balance in 60 min, indicating the hydrolysis of ACh completed within 60 min.

Further experiment was carried out to detect ACh under optimal condition. As the concentration of ACh (0.0005−6.0 mmol L^{-1}) increases (0.0005−6.0 mmol L^{-1}), more and more oxidation products (oxTMB) were produced. It is not difficult to see from Figure 4A that with the increase of the

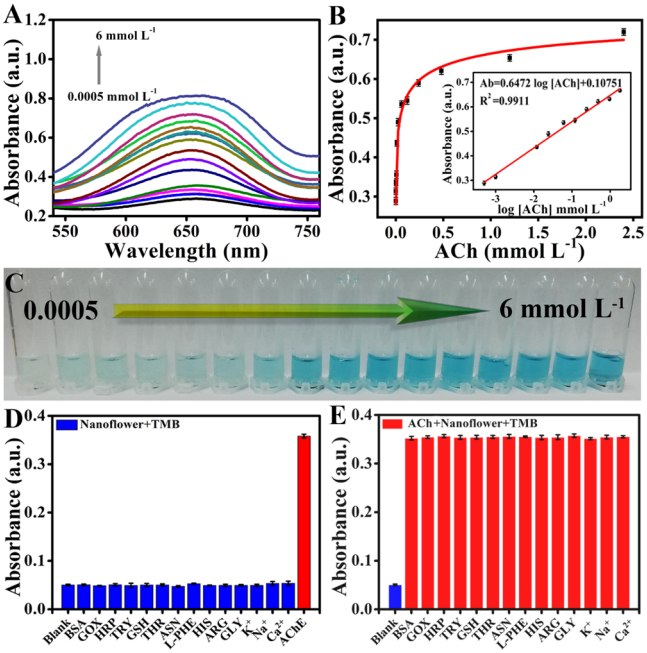

Figure 4. (A) UV−vis absorption spectra of the system with varying concentrations of ACh. (B) Trend diagram of absorbance intensity ratio with ACh concentration. The illustration shows a linear relationship between the logarithm of the ACh concentration and the intensity ratio. (C) Corresponding images taken under sunlight of mixture with different amounts of ACh. (D) Absorption value of the TMB/nanoflowers system with interfering ions and (E) absorption intensity of the ACh/nanoflowers/TMB system with the coexisting substances.

concentration of ACh, the intensity of UV−vis absorbance intensity at 652 nm increases significantly, and the color gradually turns blue (Figure 4C). Therefore, changes in absorbance intensity can be adjusted by the ACh concentration. Meanwhile, Figure 4B showed a quality linear relationship (R^2 = 0.9911) between ACh concentration and absorbance intensity. This regression equation is Ab = 0.6472 log [ACh] + 0.10751. It is worth mentioning that the detection limit (LOD) was down to 0.35 μmol L^{-1} (S/N = 3), which was more sensitive than many of the previous strategies[35] (Table S2); it is proved that the platform is suitable for ACh detection. The low LOD of this platform arises from the following distinctive features of the amplification technique: (i) protein−inorganic hybrid nanoparticles, as analogues of natural enzymes, have better stability and higher catalytic efficiency than natural enzymes and can improve the color-rendering effect and (ii) enzyme-cascade-amplification strategy is able to significantly amplify the signal of recognition, improving the detection sensitivity. Compared with a previous peroxide-based assay,[43−46] this platform for ACh possessed high stability and is easy to use. Furthermore, the response time (60 min) was quite short or comparable in contrast with the existing enzyme-based assay methods. Therefore, a low-cost and facile colorimetric platform for ACh concentration can be observed with the naked eye.

For visual biosensors, the selective recognition is very important to evaluate the practicality, especially in the point-of-care testing. Therefore, the selectivity had been studied, and the absorption peak of the common coexistence substances in biological samples such as BSA, GOX, L-phenylalanine (L-PHE), glutathione (GSH), trypsinogen (TRY), threonine (THR), asparagine (ASN), histidine (HIS), arginine (ARG), glycine (GLY), K^+, Ca^{2+}, Na^+, acetylcholine esterase (AChE), and HRP was investigated. The results are illustrated in Figure 4D; the absorbance value of the system was significantly increased after the addition of ACh, whereas the absorbance intensity did not change after the addition of these common substances, indicating that the sensing system had a good selectivity for ACh. Then, the anti-interference ability of the sensor was further studied. The response of the system to ACh was investigated in the presence of interferences. The results showed that the addition of other interfering molecules and ions had little effect on the absorbance of the ACh reaction (Figure 4E). Taken together, the established visual sensor system has good specificity and strong anti-interference ability, proving that the biological sensor is suitable for ACh detection.

To demonstrate the potential clinical use, the proposed colorimetric strategy was further applied to quantify ACh from human plasma samples that had been spiked with ACh at 0.001, 0.01, and 0.1 mmol L^{-1}. It can be seen from Table S3 with the standard addition method that the average addition recovery range is 104−119%, and the relative standard deviation was less than 5.8%, which indicates that the established sensor system is highly accurate and the ACh test reagent sample is reproducible; therefore, this sensor system has a potential applicability.

3.4. Visual Detection of ACh in Serum by a Portable Test Kit. It is well-documented that the monitoring of biomarkers (e.g., ACh) is time-consuming and expensive, especially in the early stage of disease. Thus, instant onsite visual detection of ACh on the serum sample is very significant for clinical screening and diagnosis. For this purpose, a portable visual detection kit was constructed by the use of nanoflowers/dual enzyme system to revolutionize onsite diagnosis. Owing to both low cost and easy cross-links under mild conditions, the agarose hydrogel with three-dimensional macromolecular networks that can load abundant chemical substance has been used as powerful analytical platforms in many biomedical applications.[41,47−51] In this platform, the agarose hydrogel as a robust supporter was formed by intermolecular forces without the need for potentially toxic cross-linking agents. Figure 5A illustrates the fabrication of agarose hydrogel rooted with nanoflowers as a promising platform for the detection of ACh. First, hybrid hydrogel of nanoflowers and TMB rooted into agarose were placed on a snap cap of microtube in a simple one-step protocol. To confirm the loading of nanoflower, we characterized the structure of agarose-nanoflower hybrid materials through SEM. As shown in Figure S4, the nanoflower was entrapped into the agarose hydrogel, producing a link between nanoflowers. When a clinical serum containing ACh was mixed with AChE and CHO in a microtube, the enzymatic reactions were processed to produce H_2O_2. Next, the microtube was turned upside

DOI: 10.1021/acsami.8b21571
ACS Appl. Mater. Interfaces 2019, 11, 11857−11864

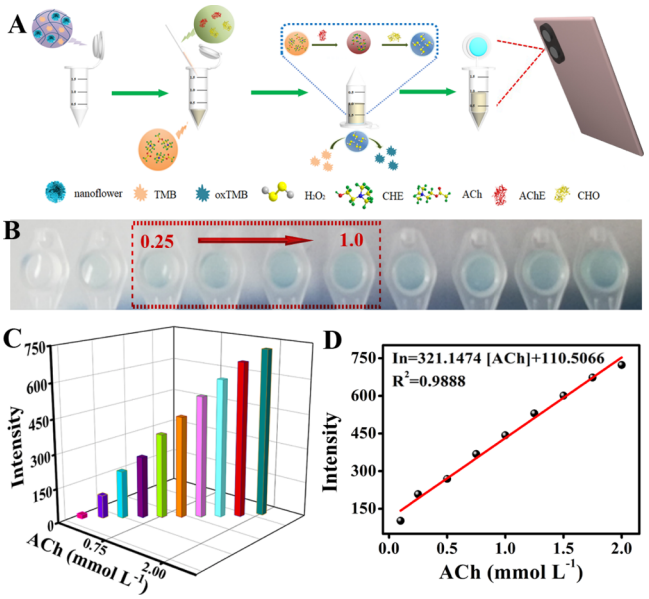

Figure 5. (A) Program for detecting ACh in serum. (I) Open the buckle cover of the kit (pale no color in the hydrogel), (II) dilute serum sample solution containing ACh was added to the kit, (III) close the kit lid and flip the kit, (IV) color of the kit changed, and (V) reverse the kit again and open the kit lid (blue color in the hydrogel). (B) Take pictures of ACh kits in different concentrations. (C) Original color image of the kit was digitally analyzed using ImageJ software to realize ACh visual detection. The concentrations of ACh are from 0.1 to 2.0 mmol L^{-1}. (D) Relationship between intensity and the concentration of ACh.

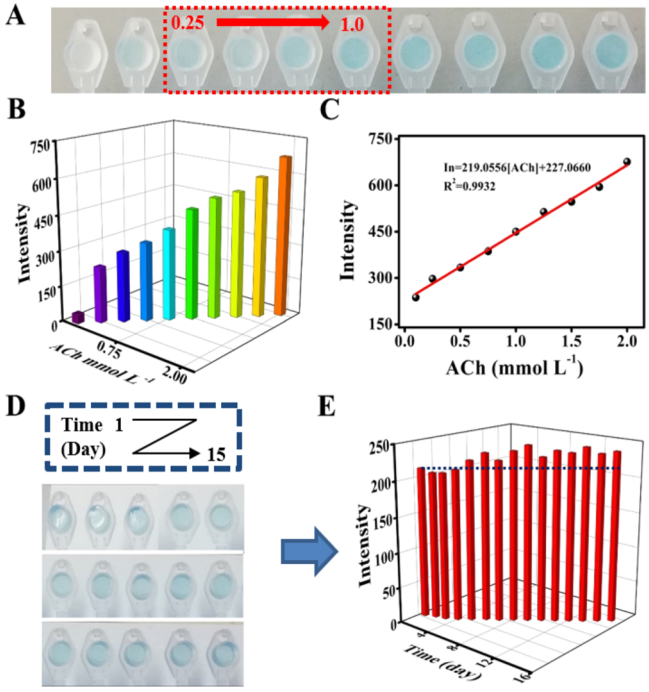

Figure 6. (A) Images of the test kits for visual detection of ACh in the serum under daylight lamp. (B) Original color image is digitized using ImageJ software. The concentrations of ACh are from 0.1 to 2.0 mmol L^{-1}. (C) Relationship between the concentration of ACh and intensity in blood serum. (D) Images of test kits for ACh within 15 days. (E) Original color image was digitized by using ImageJ software.

down to let the product diffuse into hydrogels. To observe the color change of the hydrogel, the test kit was turned upside down again and the snap cap was opened. Optical images of kits obtained by smartphone built-in cameras can be analyzed for quantitative evaluation of ACh (Figure S5). The detection of ACh in deionized water is shown in Figure 5B, and the color-gradient changes were clearly obtained. It can be seen that the naked eye detection limit was about 0.25 mmol L^{-1} of ACh. The detection results were recorded with a digital camera and were subject to quantification using ImageJ software, which produced a corresponding intensity connected with the ACh concentration. Herein, the histogram of intensity showed in Figure 5C can be considered to be another form for the color-change detection. Through analysis, we used specific data to prove that the color change had a gradient. Using the image-processing method, a good linear relation (R^2 = 0.9888) between the concentration of ACh and the intensity in the range of 0.1−2.0 mmol L^{-1} was observed for the kits (Figure 5D). These analyses proved that the nanoflower system-based kit together with the smartphone offers a portable approach for ACh detection.

The potential application was further investigated for the detection of ACh in spiked human serum samples. Figure 6A showed the color photographs of hydrogel in serum samples after adding ACh in the range from 0.1 to 2.0 mmol L^{-1}. Apparent changes of colors were identified by naked eyes. In addition, the primary color images could also be obtained and digitized by the mentioned method, as shown in Figure 6B. A good linear relationship (R^2 = 0.9887) between the intensity and the concentration of ACh in the range of 0.1−2.0 mmol L^{-1} was obtained by utilizing the image processing algorithm (Figure 6C). By means of the calibration curve, ACh can be continuously monitored by nanoflower-based measurements through image recording and analysis. It is worth pointing out that the detection sensitivity of a kit in serum samples was similar to that in deionized water, implying that serum matrix does not influence the performance of kits. Furthermore, according to previous literature,[8] the ACh level between 0.20 and 1.31 mmol L^{-1} was present in the blood of normal human beings; this indicates that the kit could meet the testing requirements of actual samples. The stability is a key parameter of point-of-care devices to evaluate the performance of strategy in practical applications. As depicted in Figure 6D, it was clearly found that the kit achieved similar color change within 15 days. As shown in Figure S6, for the blank test of the kit for 15 consecutive days, it can be clearly seen that there is no significant color change in the color of the kit. This indicates that the kit can maintain a stable state for a certain period of time, without the phenomenon of oxidation of TMB in air. Through the same analysis processes, the histogram of hue values was shown in Figure 6E. It can be easily found that the hue values had barely changed, further confirming good stability of the fabricated kit. Therefore, the portable testing kit can be used to detect ACh in real serum samples without instrumental vision. In contrast, other methods for detecting ACh have been reported previously; because the portable kit can detect ACh without complex instruments and professional operations, it has a great potential in practical applications to realize rapid detection and field detection in serum samples containing ACh.

4. CONCLUSIONS

In summary, a novel sensor for the visual detection of ACh had been constructed by using protein−inorganic hybrid nano-

DOI: 10.1021/acsami.8b21571
ACS Appl. Mater. Interfaces 2019, 11, 11857−11864

flower-based enzyme-cascade-amplification strategy. The probe relied on the catalytic ability of the nanoflower toward TMB and H_2O_2. In this sensor, protein−inorganic hybrid nanoflowers could replace natural enzymes and had advantages such as simple preparation, low cost, and high temperature resistance, which were suitable for detection in some extreme environments. This sensor could judge the content of ACh by the color displayed in the component and could be applied in practice. More importantly, a transformative idea to achieve the onsite monitoring is to fabricate portable test kits based on protein−inorganic hybrid-nanoflower-rooted agarose hydrogel platform. The integration of kit with mobile platform can perform the ease-of-use and cost-effectiveness for ACh detection, and the detection data can be easily analyzed for monitoring health care, especially in remote areas. Therefore, we believe that the nanoflower-rooted agarose hydrogel-based colorimetric assay is expected for the accurate and selective identification of ACh in real applications. What is more, our work could make efforts for the development of sensor probe design for optical sensing and the promotion of the practical application construct.

■ ASSOCIATED CONTENT

Supporting Information

The Supporting Information is available free of charge on the ACS Publications website at DOI: 10.1021/acsami.8b21571.

SEM image of nanoflowers; steady-state kinetics analysis of the nanoflower toward H_2O_2 and TMB; optimal conditions for ACh detection; SEM image of agarose hydrogel rooted with nanoflowers; stability of nanoflowers; comparison between methods; and detection results of ACh in real samples (PDF)

■ AUTHOR INFORMATION

Corresponding Authors

*E-mail: yanx@jlu.edu.cn (X.Y.).
*E-mail: lugy@jlu.edu.cn (G.L.).

ORCID

Xu Yan: 0000-0003-2152-675X
Peng Sun: 0000-0002-9509-9431
Yuehe Lin: 0000-0003-3791-7587
Geyu Lu: 0000-0002-7428-2456

Notes

The authors declare no competing financial interest.

■ ACKNOWLEDGMENTS

The authors gratefully acknowledge the financial support of the National Key Research and Development Program of China (grant number 2016YFC0207300), the National High-Tech Research and Development Program of China (grant number 2014AA06A505), the National Nature Science Foundation of China (grant numbers 61831011, 61833006, and 21806051), the Program for JLU Science and Technology Innovative Research Team (JLUSTIRT 2017TD-07), the Science and Technology Development Program of Jilin Province (grant number 2017052016JH), the Fundamental Research Funds for the Central Universities, the China Postdoctoral Science Foundation funded project (grant numbers 2017M621199 and 2018M631862), and the National Postdoctoral Program for Innovative Talents (grant number BX201700096).

■ REFERENCES

(1) Hasselmo, M. E. The Role of Acetylcholine in Learning and Memory. *Curr. Opin. Neurobiol.* **2006**, *16*, 710−715.
(2) Blokland, A. Acetylcholine: a Neurotransmitter for Learning and Memory? *Brain Res. Rev.* **1995**, *21*, 285−300.
(3) Furchgott, R. F.; Zawadzki, J. V. The Obligatory Role of Endothelial Cells in the Relaxation of Arterial Smooth Muscle by Acetylcholine. *Nature* **1980**, *288*, 373.
(4) Picciotto, M. R.; Lewis, A. S.; van Schalkwyk, G. I.; Mineur, Y. S. Mood and anxiety regulation by nicotinic acetylcholine receptors: A potential pathway to modulate aggression and related behavioral states. *Neuropharmacology* **2015**, *96*, 235−243.
(5) Sattarahmady, N.; Heli, H.; Moosavi-Movahedi, A. A. An Electrochemical Acetylcholine Biosensor Based on Nanoshells of Hollow Nickel Microspheres-carbon Microparticles-Nafion Nanocomposite. *Biosens. Bioelectron.* **2010**, *25*, 2329−2335.
(6) Wei, J.; Ren, J.; Liu, J.; Meng, X.; Ren, X.; Chen, Z.; Tang, F. An Eco-friendly, Simple, and Sensitive Fluorescence Biosensor for the Detection of Choline and Acetylcholine Based on C-dots and the Fenton Reaction. *Biosens. Bioelectron.* **2014**, *52*, 304−309.
(7) Keighron, J. D.; Wigström, J.; Kurczy, M. E.; Bergman, J.; Wang, Y.; Cans, A.-S. Amperometric Detection of Single Vesicle Acetylcholine Release Events from an Artificial Cell. *ACS Chem. Neurosci.* **2015**, *6*, 181−188.
(8) Mathew, M. S.; Baksi, A.; Pradeep, T.; Joseph, K. Choline-induced Selective Fluorescence Quenching of Acetylcholinesterase Conjugated Au@BSA clusters. *Biosens. Bioelectron.* **2016**, *81*, 68−74.
(9) Wang, H.-Y.; Lee, D. H. S.; D'Andrea, M. R.; Peterson, P. A.; Shank, R. P.; Reitz, A. B. β-Amyloid1-42Binds to α7 Nicotinic Acetylcholine Receptor with High Affinity. *J. Biol. Chem.* **2000**, *275*, 5626−5632.
(10) Calabresi, P.; Picconi, B.; Parnetti, L.; Di Filippo, M. A convergent model for cognitive dysfunctions in Parkinson's disease: the critical dopamine-acetylcholine synaptic balance. *Lancet Neurol.* **2006**, *5*, 974−983.
(11) Deutsch, S. I.; Burket, J. A.; Benson, A. D. Targeting the α7 nicotinic acetylcholine receptor to prevent progressive dementia and improve cognition in adults with Down's syndrome. *Prog. Neuro-Psychopharmacol. Biol. Psychiatry* **2014**, *54*, 131−139.
(12) Leonard, S.; Gault, J.; Hopkins, J.; Logel, J.; Vianzon, R.; Short, M.; Drebing, C.; Berger, R.; Venn, D.; Sirota, P.; Zerbe, G.; Olincy, A.; Ross, R. G.; Adler, L. E.; Freedman, R. Association of Promoter Variants in the α7 Nicotinic Acetylcholine Receptor Subunit Gene With an Inhibitory Deficit Found in Schizophrenia. *Arch. Gen. Psychiatr.* **2002**, *59*, 1085−1096.
(13) Xue, W.; Cui, T. A High-Resolution Amperometric Acetylcholine Sensor Based on Nano-Assembled Carbon Nanotube and Acetylcholinesterase Thin Films. *J. Nano Res.* **2008**, *1*, 1−9.
(14) Wang, L.; Chen, X.; Liu, C.; Yang, W. Non-enzymatic Acetylcholine Electrochemical Biosensor Based on Flower-like NiAl Layered Double Hydroxides Decorated with Carbon Dots. *Sens. Actuators, B* **2016**, *233*, 199−205.
(15) Li, H.; Guo, Y.; Xiao, L.; Chen, B. A Fluorometric Biosensor Based on H_2O_2-sensitiveNanoclusters for the Detection of Acetylcholine. *Biosens. Bioelectron.* **2014**, *59*, 289−292.
(16) Wang, C.-I.; Periasamy, A. P.; Chang, H.-T. Photoluminescent C-dots@RGO Probe for Sensitive and Selective Detection of Acetylcholine. *Anal. Chem.* **2013**, *85*, 3263−3270.
(17) Kuribayashi, M.; Tsuzuki, M.; Sato, K.; Abo, M.; Yoshimura, E. A Rapid Analytical Method for Free Choline by LC and Its Application for Bacterial Culture Medium Samples. *Chromatographia* **2007**, *67*, 339−341.
(18) Qian, J.; Yang, X.; Jiang, L.; Zhu, C.; Mao, H.; Wang, K. Facile Preparation of Fe_3O_4 Nanospheres/reduced Graphene Oxide Nanocomposites with High Peroxidase-like Activity for Sensitive and Selective Colorimetric Detection of Acetylcholine. *Sens. Actuators, B* **2014**, *201*, 160−166.
(19) Burmeister, J. J.; Pomerleau, F.; Huettl, P.; Gash, C. R.; Werner, C. E.; Bruno, J. P.; Gerhardt, G. A. Ceramic-based Multisite

Microelectrode Arrays for Simultaneous Measures of Choline and Acetylcholine in CNS. *Biosens. Bioelectron.* **2008**, *23*, 1382−1389.
(20) Zayats, M.; Kharitonov, A. B.; Pogorelova, S. P.; Lioubashevski, O.; Katz, E.; Willner, I. Probing Photoelectrochemical Processes in Au−CdS Nanoparticle Arrays by Surface Plasmon Resonance: Application for the Detection of Acetylcholine Esterase Inhibitors. *J. Am. Chem. Soc.* **2003**, *125*, 16006−16014.
(21) Chauhan, N.; Chawla, S.; Pundir, C. S.; Jain, U. An Electrochemical Sensor for Detection of Neurotransmitter-acetylcholine Using Metal Nanoparticles, 2D Material and Conducting Polymer Modified Electrode. *Biosens. Bioelectron.* **2017**, *89*, 377−383.
(22) Liu, P.; Yang, X.; Sun, S.; Wang, Q.; Wang, K.; Huang, J.; Liu, J.; He, L. Enzyme-free Colorimetric Detection of DNA by Using Gold Nanoparticles and Hybridization Chain Reaction Amplification. *Anal. Chem.* **2013**, *85*, 7689−7695.
(23) Chen, X.; Chen, J.; Wang, F.; Xiang, X.; Luo, M.; Ji, X.; He, Z. Determination of Glucose and Uric acid with Bienzyme Colorimetry on Microfluidic Paper-based Analysis Devices. *Biosens. Bioelectron.* **2012**, *35*, 363−368.
(24) Kasahara, Y.; Ashihara, Y. Colorimetry of angiotensin-I converting enzyme activity in serum. *Clin Chem* **1981**, *27*, 1922−1925.
(25) Dutta, S.; Ray, C.; Mallick, S.; Sarkar, S.; Sahoo, R.; Negishi, Y.; Pal, T. A Gel-Based Approach To Design Hierarchical CuS Decorated Reduced Graphene Oxide Nanosheets for Enhanced Peroxidase-like Activity Leading to Colorimetric Detection of Dopamine. *J. Phys. Chem. C* **2015**, *119*, 23790−23800.
(26) Boppart, S. A.; Richards-Kortum, R. Point-of-care and Point-of-procedure Optical Imaging Technologies for Primary Care and Global Health. *Sci. Transl. Med.* **2014**, *6*, 253rv2.
(27) Srinivasan, B.; Tung, S. Development and Applications of Portable Biosensors. *J. Lab. Autom.* **2015**, *20*, 365−389.
(28) Dong, Y.-l.; Zhang, H.-g.; Rahman, Z. U.; Su, L.; Chen, X.-j.; Hu, J.; Chen, X.-g. Graphene oxide-Fe3O4 magnetic nanocomposites with peroxidase-like activity for colorimetric detection of glucose. *Nanoscale* **2012**, *4*, 3969−3976.
(29) Xu, X.; Han, M. S.; Mirkin, C. A. A Gold-Nanoparticle-Based Real-Time Colorimetric Screening Method for Endonuclease Activity and Inhibition. *Angew. Chem.* **2007**, *119*, 3538−3540.
(30) Cui, R.; Han, Z.; Zhu, J.-J. Helical Carbon Nanotubes: Intrinsic Peroxidase Catalytic Activity and Its Application for Biocatalysis and Biosensing. *Chem.—Eur. J.* **2011**, *17*, 9377−9384.
(31) Zheng, X.; Liu, Q.; Jing, C.; Li, Y.; Li, D.; Luo, W.; Wen, Y.; He, Y.; Huang, Q.; Long, Y.-T.; Fan, C. Catalytic Gold Nanoparticles for Nanoplasmonic Detection of DNA Hybridization. *Angew. Chem., Int. Ed. Engl.* **2011**, *50*, 11994−11998.
(32) Gao, L.; Zhuang, J.; Nie, L.; Zhang, J.; Zhang, Y.; Gu, N.; Wang, T.; Feng, J.; Yang, D.; Perrett, S.; Yan, X. Intrinsic Peroxidase-like Activity of Ferromagnetic Nanoparticles. *Nat. Nanotechnol.* **2007**, *2*, 577−583.
(33) Asati, A.; Santra, S.; Kaittanis, C.; Nath, S.; Perez, J. M. Oxidase-like Activity of Polymer-coated Cerium Oxide Nanoparticles. *Angew. Chem., Int. Ed. Engl.* **2009**, *48*, 2308−2312.
(34) Song, Y.; Qu, K.; Zhao, C.; Ren, J.; Qu, X. Graphene Oxide: Intrinsic Peroxidase Catalytic Activity and its Application to glucose detection. *Adv. Mater.* **2010**, *22*, 2206−2210.
(35) Xia, N.; Wang, Q.; Liu, L. Nanomaterials-based Optical Techniques for the Detection of Acetylcholinesterase and Pesticides. *Sensors* **2014**, *15*, 499−514.
(36) Lin, Y.; Chapman, R.; Stevens, M. M. Label-Free Multimodal Protease Detection Based on Protein/Perylene Dye Coassembly and Enzyme-Triggered Disassembly. *Anal. Chem.* **2014**, *86*, 6410−6417.
(37) Huang, Y.; Ran, X.; Lin, Y.; Ren, J.; Qu, X. Self-assembly of an Organic-inorganic Hybrid Nanoflower as an Efficient Biomimetic Catalyst for Self-activated Tandem Reactions. *Chem. Commun.* **2015**, *51*, 4386−4389.
(38) Jiao, J.; Xin, X.; Wang, X.; Xie, Z.; Xia, C.; Pan, W. Self-assembly of biosurfactant-inorganic hybrid nanoflowers as efficient catalysts for degradation of cationic dyes. *RSC Adv.* **2017**, *7*, 43474−43482.
(39) Lin, Y.; Li, Z.; Chen, Z.; Ren, J.; Qu, X. Mesoporous Silica-encapsulated Gold Nanoparticles as Artificial Enzymes for Self-activated Cascade Catalysis. *Biomaterials* **2013**, *34*, 2600−2610.
(40) Yi, Y.; Zhu, G.; Liu, C.; Huang, Y.; Zhang, Y.; Li, H.; Zhao, J.; Yao, S. A Label-free Silicon Quantum Dots-based Photoluminescence Sensor for Ultrasensitive Detection of Pesticides. *Anal. Chem.* **2013**, *85*, 11464−11470.
(41) Xia, N.; Zhang, Y.; Chang, K.; Gai, X.; Jing, Y.; Li, S.; Liu, L.; Qu, G. Ferrocene-phenylalanine hydrogels for immobilization of acetylcholinesterase and detection of chlorpyrifos. *J. Electroanal. Chem.* **2015**, *746*, 68−74.
(42) Peters, G. M.; Skala, L. P.; Plank, T. N.; Hyman, B. J.; Manjunatha Reddy, G. N.; Marsh, A.; Brown, S. P.; Davis, J. T. A G_4·K^+ Hydrogel Stabilized by an Anion. *J. Am. Chem. Soc.* **2014**, *136*, 12596−12599.
(43) Lin, Y.; Yu, P.; Mao, L. A Multi-Enzyme Microreactor-based Online Electrochemical System for Selective and Continuous Monitoring of Acetylcholine. *Analyst* **2015**, *140*, 3781−3787.
(44) Valekar, A. H.; Batule, B. S.; Kim, M. I.; Cho, K.-H.; Hong, D.-Y.; Lee, U.-H.; Chang, J.-S.; Park, H. G.; Hwang, Y. K. Novel Amine-Functionalized Iron Trimesates with Enhanced Peroxidase-like Activity and Their Applications for the Fluorescent Assay of Choline and Acetylcholine. *Biosens. Bioelectron.* **2018**, *100*, 161−168.
(45) Martín-Barreiro, A.; de Marcos, S.; de la Fuente, J. M.; Grazú, V.; Galbán, J. Gold Nanocluster Fluorescence as an Indicator for Optical Enzymatic Nanobiosensors: Choline and Acetylcholine Determination. *Sens. Actuators, B* **2018**, *277*, 261−270.
(46) Akhtar, M. H.; Hussain, K. K.; Gurudatt, N. G.; Shim, Y.-B. Detection of Ca^{2+}-Induced Acetylcholine Released from Leukemic T-cells Using an Amperometric Microfluidic Sensor. *Biosens. Bioelectron.* **2017**, *98*, 364−370.
(47) Giménez, C.; Climent, E.; Aznar, E.; Martínez-Máñez, R.; Sancenón, F.; Marcos, M. D.; Amorós, P.; Rurack, K. Towards chemical communication between gated nanoparticles. *Angew. Chem. Int. Ed.* **2014**, *53*, 12629−12633.
(48) Al Sulaiman, D.; Chang, J. Y. H.; Ladame, S. Subnanomolar Detection of Oligonucleotides through Templated Fluorogenic Reaction in Hydrogels: Controlling Diffusion to Improve Sensitivity. *Angew. Chem., Int. Ed.* **2017**, *56*, 5247−5251.
(49) Gogoi, N.; Barooah, M.; Majumdar, G.; Chowdhury, D. Carbon Dots Rooted Agarose Hydrogel Hybrid Platform for Optical Detection and Separation of Heavy Metal Ions. *ACS Appl. Mater. Interfaces* **2015**, *7*, 3058−3067.
(50) Singh, Y. P.; Bhardwaj, N.; Mandal, B. B. Potential of Agarose/Silk Fibroin Blended Hydrogel for in Vitro Cartilage Tissue Engineering. *ACS Appl. Mater. Interfaces* **2016**, *8*, 21236−21249.
(51) Lin, T.; Zhong, L.; Song, Z.; Guo, L.; Wu, H.; Guo, Q.; Chen, Y.; Fu, F.; Chen, G. Visual Detection of Blood Glucose Based on Peroxidase-like Activity of WS_2 Nanosheets. *Biosens. Bioelectron.* **2014**, *62*, 302−307.

DOI: 10.1021/acsami.8b21571
ACS Appl. Mater. Interfaces 2019, 11, 11857−11864